

BUBBLES NEAR THE NULL FINAL KELVIN IMPULSE STATE

Emil-Alexandru BRUJAN

Department of Hydraulics, University Polytechnica, Spl. Independentei 313, 77206 Bucharest, Romania,
E-mail: eabrujan@hydrop.pub.ro

The dynamics of a buoyant bubble near a rigid boundary at the null final Kelvin impulse state is investigated numerically by using a boundary integral method. The results of the numerical calculations provided the bubble profiles and the pressure contours in the liquid surrounding the bubble. Three cases are chosen to typify the jetting behaviour at the null final Kelvin impulse state: (i) formation of an asymmetric annular jet leading to bubble splitting; (ii) formation of an asymmetric annular jet and a high-speed axial jet directed away from the boundary, and (iii) formation of two opposite high-speed axial jets directed towards the bubble centre as a consequence of a more symmetric but weaker annular jet in the initial stage of bubble collapse. The complex behaviour is attributed to a slight difference between the strength of the opposite forces during bubble collapse. The present results indicate that the jetting behaviour in the neighbourhood of the neutral bubble collapse can be adequately described by the Kelvin impulse itself, but evaluated during the collapse phase of the bubble. Its direction determines the position of the annular jet in the initial phase of the collapse while its magnitude indicates the degree of asymmetry and the intensity of the annular jet. Both factors are essential in estimating the final fate of the bubble at the neutral collapse state. Far from this state, the final Kelvin impulse is a valuable tool in predicting the migratory characteristics of the bubble and the direction of the axial jet developed during bubble collapse.

1. INTRODUCTION

Since the classic work of Rayleigh [1], the collapse of a cavity has been treated with various degrees of sophistication. Rayleigh analysed the collapse of an empty spherical bubble in a liquid of infinite extent under hydrostatic pressure. Other works have included the effects of surface tension, viscosity and compressibility (see, for example, Prosperetti and Lezzi [2] and the references therein). Kornfeld and Suvorov [3] were the first to suggest that bubbles might collapse asymmetrically and produced a jet. The asymmetry of the collapse is a result of a pressure gradient across the bubble. In the case when this pressure gradient is provided by a rigid boundary, a jet forms which is directed onto the surface [4]. The most significant parameter affecting the dynamical properties of the jet is the non-dimensional stand-off, defined as the distance of the initial location of the bubble from the boundary scaled by the maximum bubble radius, which is denoted by γ [5], [6].

In addition to the pressure gradient generated by the rigid boundary, a large pulsating, buoyant bubble is subjected to a second pressure gradient induced by the gravitational field. Depending on the direction and the relative strength of the pressure gradients a large variety of the jetting behaviour was identified which includes the formation of an annular jet and axial jets directed towards and away from the boundary. Classic examples are given in the papers by Blake et al. [5] and Best and Kucera [7]. The evidence of the numerical computations presented in these papers also indicates that the direction of the jet and the direction of the Kelvin impulse at the end of the collapse (final Kelvin impulse state) are closely correlated. A less understood aspect of the bubble dynamics is the jetting behaviour at the null final Kelvin impulse state. This case is particularly interesting because the opposite forces acting on the bubble motion, namely the pressure-gradient force directed towards the boundary and the buoyancy repulsive force, lead to a near zero Kelvin impulse at the end of bubble collapse.

In this paper, the dynamics of a pulsating, buoyant bubble situated above a rigid boundary at the null final Kelvin impulse state is investigated numerically by using a boundary integral method. The results of the

numerical computations provided the bubble profiles and the pressure contours in the liquid surrounding the bubble. We found a complex jetting behaviour which depends strongly on the initial location of the bubble from the boundary. At small γ -values, an asymmetric annular jet is formed leading to bubble splitting. At intermediate γ -values, an annular asymmetric jet and an axial jet directed away from the boundary are observed. At large γ -values, two axial jets directed towards the bubble centre are developed during the collapse phase of the bubble as a consequence of a more symmetric but weaker annular jet in the initial phase of bubble collapse. Each jet is further accelerated during the final stage of the bubble collapse by a high-pressure region that develops when the bubble wall is already indented. The complex jetting behaviour is attributed to a difference between the strength of the opposite forces during the collapse phase of the bubble.

We believe that the present results are interesting in two complementary ways. First, they reveal the complex jetting behaviour of a bubble situated in two opposite pressure gradients in the neighbourhood of the null final Kelvin impulse state. Secondly, they offer an insight into the applicability of the concept of the Kelvin impulse in predicting the dynamical characteristics of a bubble at the neutral collapse state.

2. MATHEMATICAL FORMULATION

The fluid mechanics of energetic, pulsating, buoyant bubbles are dominated by inertial effects because of the high velocities and short time scales leading to very high Reynolds number flows. Pressures are typically large so that the surface tension effects are best ignored. However, buoyancy forces are important in this case. We define a parameter δ as follows:

$$\delta = \left(\frac{\rho g R_m}{\Delta p} \right)^{1/2} \quad (1)$$

with ρ the density of the fluid, g gravitational acceleration, R_m maximum bubble radius, and $\Delta p = p_\infty - p_v$ the pressure scale obtained from the difference between the ambient pressure at the point of bubble generation and the vapour pressure. Physically, δ corresponds to the ratio of the velocity of the bubble associated with motion to buoyancy, $(gR_m)^{1/2}$, to the characteristic velocity of bubble growth or collapse $(\Delta p/\rho)^{1/2}$. In the calculations that follow, this latter velocity will be used to calculate velocities, R_m to scale length and Δp pressures.

The liquid volume Ω surrounding the bubble is assumed inviscid and incompressible, and the motion irrotational leading to the potential flow equations with the velocity represented by the gradient of a potential

$$\mathbf{u} = \nabla\phi, \quad \nabla^2\phi = 0 \quad (2)$$

The pressure inside the cavity is assumed to be uniform and consists of a constant vapour pressure and a volume-dependent non-condensable gas pressure. A simple adiabatic model is used for the variation of cavity pressure, p_c , giving

$$p_c = p_v + p_0 (V_0/V)^\kappa, \quad (3)$$

where p_0 is the initial pressure of the non-condensable gas inside the bubble (corresponding to a bubble volume V_0) and κ is the ratio of specific heats. The assumption of a uniform gas pressure is likely to be inaccurate over the last few percent of the collapse time but one would not expect this circumstance to induce order-of-magnitude errors in the results.

The dynamic boundary condition on the bubble surface, $\partial\Omega_b$, can be written as

$$\frac{D\phi}{Dt} = \frac{1}{2} |\nabla\phi|^2 - \alpha \left(\frac{V_0}{V} \right)^\kappa - \delta^2 (z - \gamma) + 1, \quad (4)$$

where $\alpha = p_0/\Delta p$ is the strength parameter. This parameter provides a measure of the magnitude of the initial partial pressure exerted by the non-condensable bubble contents. In the case of explosion bubbles this pressure is high and drives the oscillation of the bubble. The term D/Dt denotes the material derivative and

Cartezian coordinates are chosen such that gravity acts in the negative z -direction. The kinematic condition stipulates that

$$\frac{D\mathbf{x}}{Dt} = \nabla\phi \quad (5)$$

The solution of (2) may be written in terms of an integral equation

$$\frac{1}{2}\phi(\mathbf{x}') = \int_{\partial\Omega} \left(\frac{\partial\phi(\mathbf{x})}{\partial n} G(\mathbf{x}, \mathbf{x}') - \phi(\mathbf{x}) \frac{\partial G(\mathbf{x}, \mathbf{x}')}{\partial n} \right) dS, \quad (6)$$

where S is the bubble surface and $G(\mathbf{x}, \mathbf{x}')$ is the Green's function

$$G(\mathbf{x}, \mathbf{x}') = \frac{1}{4\pi|\mathbf{x} - \mathbf{x}'|} + \frac{1}{4\pi|\mathbf{x} - \mathbf{x}''|} \quad (7)$$

with $\mathbf{x}, \mathbf{x}' \in \partial\Omega$ and \mathbf{x}'' the image of \mathbf{x}' reflected about the boundary. This form of the Green function satisfies the no-flow condition through the rigid boundary.

Initial conditions are dependent on the particular application. For example, direct modelling of the temporal evolution and spatial distribution of the energy deposition during detonation is complicated, and details depends strongly on the type and geometry of the explosive charges [8]. We therefore neglect the details of the detonation process and assume that the bubble originates from a small spherical cavity of radius R_0 , wall velocity v_0 , and internal pressure p_0 which subsequently grows to many times its initial volume. The constants in the above equations are: density of water $\rho_0 = 998 \text{ kg/m}^3$, polytropic exponent $\kappa = 1.4$, vapour pressure $p_v = 2.35 \text{ kPa}$, and static ambient pressure $p_\infty = 100 \text{ kPa}$. An arbitrary starting condition at $t = 0$ is chosen for the numerical computations, using the Rayleigh-Plesset equation with the initial non-dimensional radius of the cavity $R_0 = 0.1383$, the initial pressure $\alpha = 100$, and the initial velocity on the free surface $v_0 = 10$. It should be noted here that different values of the initial pressure and radial velocity show the same gross structure of bubble dynamics at null final Kelvin impulse state, with just shifted values in the γ - δ parameter space. This has been confirmed by some trial calculations with v_0 in the range 1 to 100 and α up to 1000.

3. KELVIN IMPULSE

The concept of the Kelvin impulse, which was applied to bubble dynamics by Benjamin and Ellis [9], provides a useful theoretical framework for interpreting the behaviour of a bubble near boundaries. The Kelvin impulse can be interpreted as a linear impulse of the bubble if one attributes a virtual mass to the bubble which corresponds to the liquid mass moving around the cavity. Since axial jets are always associated with bubble migration in the direction of the jet, it was suggested that their occurrence and direction can be predicted by analysing the Kelvin impulse at the end of the bubble collapse [5], [7], [9].

The Kelvin impulse of a cavity is defined as

$$\mathbf{I} = \int_{S_b} \phi \mathbf{n} dS \quad (8)$$

where S_b is the surface of the bubble. The rate of change of the Kelvin impulse is given by

$$\frac{d\mathbf{I}}{dt} = \mathbf{F}^\Sigma + \mathbf{F}^g, \quad (9)$$

with

$$\mathbf{F}^\Sigma = - \int_{S_b} \left\{ \frac{1}{2} |\nabla\phi|^2 \mathbf{n} - \frac{\partial\phi}{\partial n} \nabla\phi \right\} dS, \quad (10)$$

and

$$\mathbf{F}^g = \delta^2 V \mathbf{e}_z, \quad (11)$$

\mathbf{e}_z being a unit vector in the positive z -direction. \mathbf{F}^g is the buoyancy force and \mathbf{F}^Σ is the pressure-gradient force exerted by the boundary. These expressions can be derived by using the fact that the hydrodynamic force, \mathbf{F}_h , on the bubble is zero, where

$$\mathbf{F}_h = -\frac{d\mathbf{I}}{dt} - \int_{S_b} \left\{ \frac{1}{2} |\nabla\phi|^2 \mathbf{n} - \frac{\partial\phi}{\partial n} \nabla\phi \right\} dS + \delta^2 V \mathbf{e}_z \quad (12)$$

It is evident from (9) that the Kelvin impulse is a function of time, starting from zero at inception and changing sign during the lifetime of the bubble depending on the relative strength of the forces acting on the bubble motion. The interesting feature of (9) is the existence of a null Kelvin impulse state defined by $I = \int (\mathbf{F}^\Sigma + \mathbf{F}^g) dt = 0$ at the end of the bubble lifetime. It is at this state that the strength of the competing pressure-gradient and buoyancy forces is equal and the centroid of the bubble maintains its initial position.

A comment on the calculation of the Kelvin impulse is appropriate here. When the bubble is initiated very close to the rigid boundary the computations break down before the bubble reaches the minimum volume and, therefore, the final Kelvin impulse of the bubble cannot be accurately calculated. In this case, the null final Kelvin impulse state of the bubble is estimated by considering the centroid position in a very late stage of bubble collapse. With increasing the initial distance between bubble and boundary the computations describe better the final stages of bubble collapse and the calculated value of the final Kelvin impulse becomes more accurate.

4. RESULTS

4.1. Final Kelvin impulse, bubble migration and jet formation

Figure 1 shows the relation between jet formation, centroid migration and final Kelvin impulse for a stand-off of $\gamma = 1$. When the magnitude of the opposing forces is equal, the final Kelvin impulse is zero and a symmetric annular jet is observed in a late collapse stage. An asymmetric annular jet develops when the strength of the opposing forces are not equally strong. The asymmetric annular jet is located at the bubble part closer to the boundary when the final Kelvin impulse is directed away from the boundary ($I(t_c) > 0$), while if it is directed towards the boundary ($I(t_c) < 0$) the annular jet will be located at the bubble part far from the boundary. Obviously, the larger the absolute value of the final Kelvin impulse, the more asymmetric is the position of the annular jet during bubble collapse. In the very late stages of the collapse, the annular jet leads to bubble splitting and the generation of two high-speed axial jets in opposite direction. These features have been also observed for motion between parallel plates [10], in an axisymmetric stagnation flow towards a rigid boundary [11], and near an elastic boundary [12]. In the limit, however, where one of the opposite forces assumes dominance, only one axial jet is formed and the bubble migrates in the direction of the dominant force. Later in the collapse phase the axial jet penetrates the opposite bubble wall and the bubble takes a toroidal shape.

A very interesting phenomenon is observed for a stand-off of $\gamma = 2$ (figure 2). The transition from jet formation directed downwards to jet formation directed upwards, as the relative strengths of the buoyancy and pressure-gradient forces change, consists of two axial jets directed towards the bubble centre. At the null final Kelvin impulse state of the bubble the upper jet is faster and thinner than the lower one. At larger values of the final Kelvin impulse the lower jet becomes dominant, while the dominance of the upper jet is preserved at smaller values of the final Kelvin impulse. Similar results have been reported for the motion of a bubble situated in a rearward stagnation-point flow near a rigid boundary [5]. We further note that, in both examples, the direction of the final Kelvin impulse coincides with the direction of bubble migration.

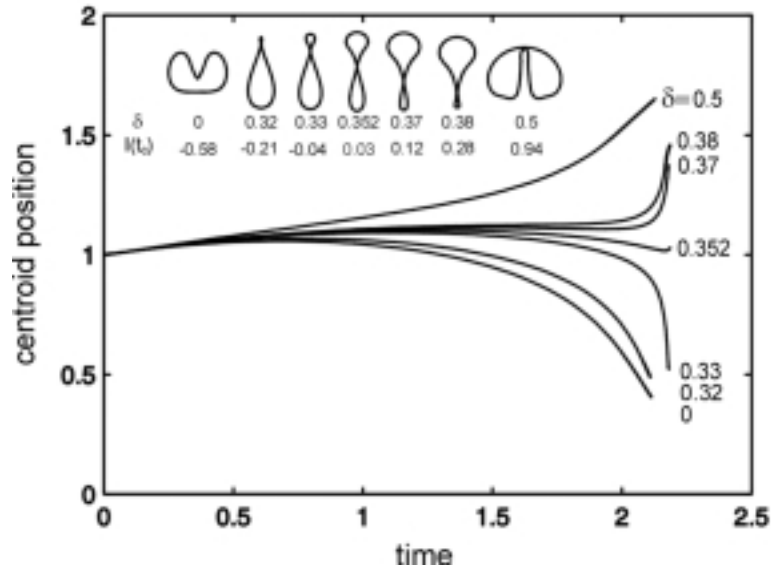


Figure 1. Centroid position of a bubble situated above a rigid boundary for $\gamma = 1$ and different values of the buoyancy parameter. The computed bubble shape in the final collapse stage is also illustrated. The value of the Kelvin impulse at the end of the collapse is given below each bubble shape. The null final Kelvin impulse state of the bubble is considered to occur for $\delta = 0.352$, although the calculated value of the final Kelvin impulse is 0.03. It is at this δ -value that the centroid position in the very late collapse stage is close to the initial distance between bubble and boundary. Slightly larger or smaller values of δ result in bubble migration away-from and towards the boundary, respectively.

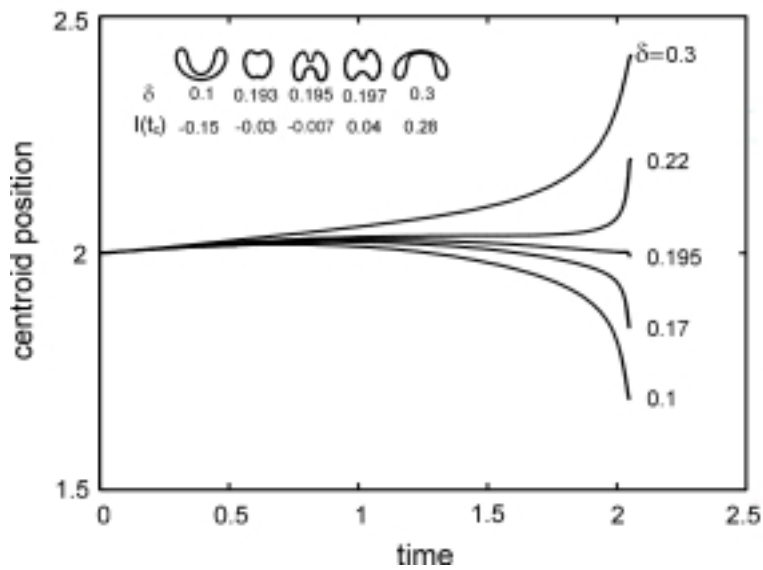


Figure 2. Centroid position of a bubble situated above a rigid boundary for $\gamma = 2$ and different values of the buoyancy parameter. The computed bubble shape in the final collapse stage is also illustrated. The value of the Kelvin impulse at the end of the collapse is given below each bubble shape.

4.2. Bubble dynamics at the null final Kelvin impulse state

In this section we give representative examples of the dynamics of a pulsating, buoyant bubble close to a rigid boundary and at the null final Kelvin impulse state. Three typical cases are identified as the initial location of the bubble from the rigid boundary is increased: (i) formation of an asymmetric annular jet leading to bubble splitting; (ii) formation of an asymmetric annular jet and an axial jet directed away from the boundary, and (iii) formation of two opposite axial jets directed towards the bubble centre. Later below we shall demonstrate that this is the only possible jetting behaviour a pulsating buoyant bubble situated near a rigid boundary can have at the null final Kelvin impulse state.

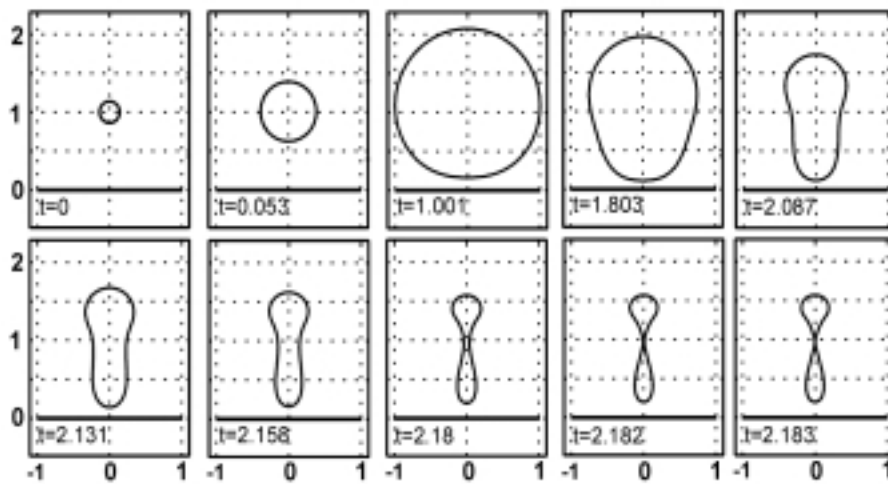


FIGURE 3. Bubble dynamics at the null final Kelvin impulse state for $\gamma = 1$ and $\delta = 0.352$.

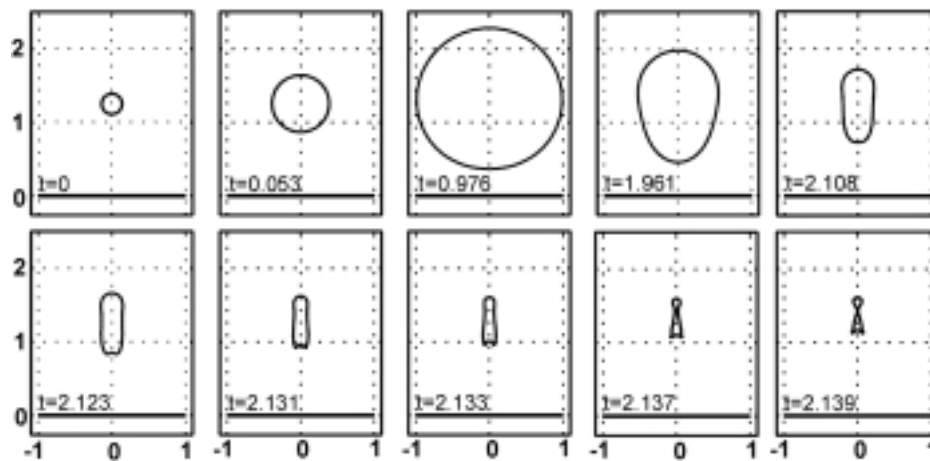


Figure 4. Bubble dynamics at the null final Kelvin impulse state for $\gamma = 1.25$ and $\delta = 0.292$.

Figure 3 illustrates the temporal development of the bubble shape when the values of the stand-off and buoyancy parameter are $\gamma = 1$ and $\delta = 0.352$. Although during the initial growth phase the bubble keeps its spherical symmetry, at maximum volume it becomes flattened in a direction parallel to the boundary. Once the oblate shape of the bubble is formed ($t = 1.001$), it collapses from its sides leading to the production of an annular flow which is most pronounced around the surface of the bubble closer to the rigid boundary. Therefore, an "egg-timer" shape of the bubble develops in a later stage of the collapse (frames 5-7). An

additional factor contributing to the formation of the "egg-timer" shape is the low-pressure region between the collapsing cavity and the boundary which holds the bubble wall facing the boundary. The maximum velocity of the annular jet is 28 (approximately 280 m/s in absolute value) and is reached in the final stage of bubble collapse. At time $t = 2.183$, pinch-off is observed to occur and the bubble splits in two. Beyond this time the computational scheme cannot proceed. Had the calculations been allowed to continue, two high-speed axial jets emanating from the high-curvature regions of closure would be formed, the lower of which would strike the boundary with an ultra high velocity.

In figure 4 ($\gamma = 1.25$, $\delta = 0.292$), the bubble is situated further from the rigid boundary expanding more symmetrically towards maximum volume. In this case, the asymmetric annular flow leads to the formation of a "cone-shaped" bubble region at the side next to the boundary. The collapse of this high curvature region of the bubble subsequently produces an axial liquid jet directed away from the boundary (frames 6-10). The intensity of the annular jet is, however, high enough that the jet manifests over the whole collapse phase of the bubble. Therefore, both an annular and an axial jet are observed at the conclusion of bubble collapse. Interestingly, the location of the annular jet moves during the collapse phase from the bubble side nearest to the boundary to its side far from the boundary. As before, at closure of the neck, pinch-off occurs forming two high-speed axial jets in opposite directions. The damage potential of the high-speed liquid jet that crosses the cavity closer to the boundary is certainly lower than in the previous case because the jet is strongly decelerated on its way to the boundary by the axial jet developed at the bubble pole closer to the boundary and by the thicker liquid layer between bubble and boundary.

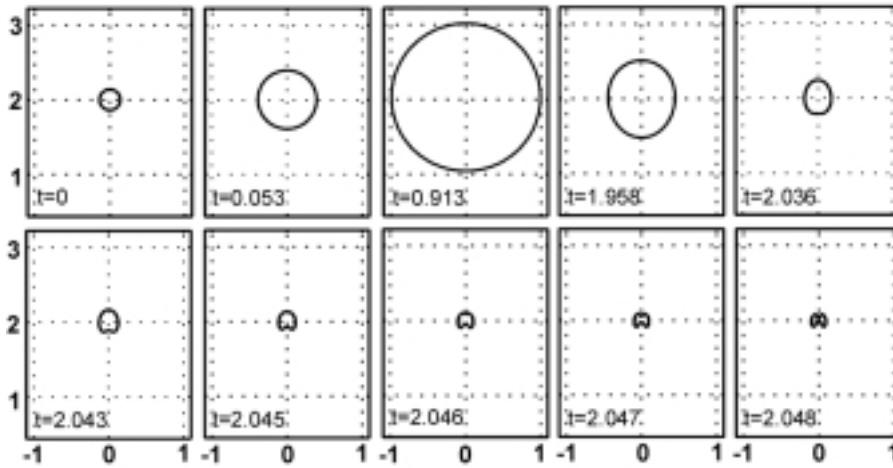


Figure 5. Bubble dynamics at the null final Kelvin impulse state for $\gamma = 2$ and $\delta = 0.195$.

When the bubble is initiated further from the boundary (figure 5; $\gamma = 2$, $\delta = 0.195$), it retains much of its spherical symmetry at the maximum expansion. In this case the flow field is more symmetrical and the formation of an annular flow occurs around the bubble equator. Therefore, the bubble acquires the form of a prolate spheroid during the initial collapse phase (frames 4 and 5). Subsequently, two axial liquid jets directed towards bubble centre develop at the bubble poles. The jet directed away from the boundary develops first as a result of a higher curvature of the bubble wall close to the boundary. We note that whereas the maximum velocity of the axial jet directed towards the boundary is 30 the corresponding value for the axial jet directed away from the boundary is about 18. The fluid speed upon collapse is so high that both jets penetrate the bubble sufficiently that the bubble does not rebound in connected form. The damage capability of the bubble is even smaller in this case, on one hand, because the bubble is too far from the boundary at the end of the collapse and, on the other hand, the axial jets interfere with one another in the final collapse stage. The formation of two opposite axial jets was also observed experimentally during the collapse of cylindrical bubbles in a liquid of infinite extent [13].

The rigid boundary leads to a prolongation of the collapse time of the bubble and to a decrease of the maximum pressure in the liquid surrounding the bubble. For large γ -values, the collapse is almost spherical and the axial jets develop only in a very late stage of the collapse. Therefore, the liquid moves almost

radially towards the collapse centre, leading to a violent collapse with a strong compression of the bubble contents. For small γ -values, the annular flow is dominant while the upper and lower sides of the bubble are almost motionless (figure 3, frames 6-10). Thus kinetic energy is associated with this motion, so the bubble content becomes less compressed than in the case of large γ -values (compare the minimum bubble sizes for the cases illustrated in figures 3 and 5) and the pressure amplitude in the surrounding liquid is diminished.

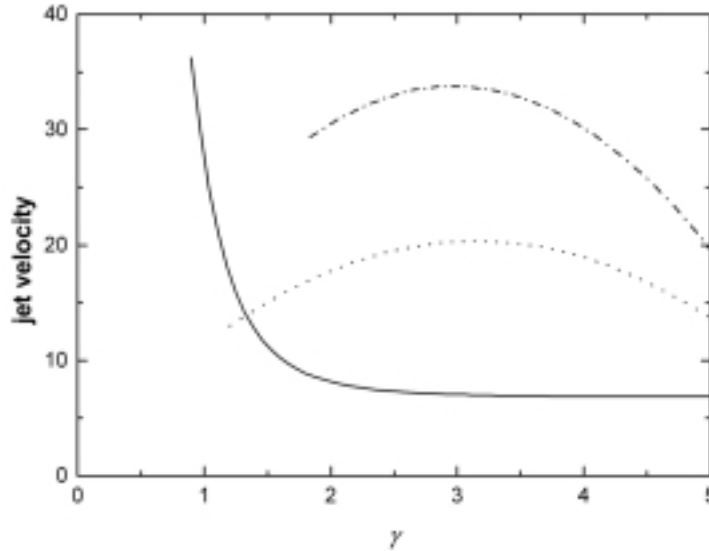


Figure 6. Velocity of the annular jet (solid line) and axial jets directed towards the bubble centre (upper jet: dash and dot line, lower jet: dotted line) developed during bubble collapse at the null final Kelvin impulse state.

Figure 6 shows the maximum velocity of the annular jet and axial jets directed towards and away from the rigid boundary at the null final Kelvin impulse state as a function of the stand-off parameter γ . A first qualitative comment is that the maximum velocity reached by the annular jet is strikingly high with values of up to 36 at $\gamma = 0.9$. This value could be even higher for smaller γ -values. We note, however, that the numerical code ceases to be valid for $\gamma < 0.9$ because of the very thin liquid layer between bubble and boundary. The annular jet velocity becomes smaller when γ is increased so that at $\gamma = 5$ the maximum jet velocity is about 6.5. It is worth noting here that, for $\gamma = 0.9$, the maximum velocity of the annular jet is reached at the end of the collapse. With increasing γ , the maximum velocity of this jet is reached in an earlier stage of the collapse. On the other hand, each axial jet is characterised by a critical value of γ at which the maximum velocity of the jet attains the highest value. The axial jet directed away from the boundary is initiated at smaller γ -values and is relatively thicker and slower. It was found that an increase with one order of magnitude of the strength parameter results in an increase of the maximum velocity of the jets with a factor of 6. At these high values the assumption of liquid incompressibility adopted in the present model is no longer justified. These results give, however, an indication about how violent the collapse can be when the bubble oscillates at the null final Kelvin impulse state.

4.3. Jetting behaviour as a function of γ and δ

Figure 7 gives an overview of the jetting behaviour as a function of the normalized distance between bubble and boundary γ and the buoyancy parameter δ . The solid line denotes the null final Kelvin impulse state where the bubble centroid maintains its initial position at the end of the collapse (neutral bubble collapse). States described by points lying above the null final Kelvin impulse curve ($I(t_c) > 0$) correspond to bubble migration away from the boundary, while points lying below the null final Kelvin impulse curve ($I(t_c) < 0$), correspond to bubble migration towards the boundary. The zones where only one axial jet develops during bubble collapse are separated by regions centred around the null final Kelvin impulse curve with a complex jetting behaviour. For small γ -values, an annular jet develops leading to bubble splitting and the formation of two axial jets directed towards and away from the boundary. The bubble achieves an oblate

shape in the early collapse phase and collapses faster from the sides in a later stage. This leads to the formation of a strong annular jet which finally separates the upper and lower parts of the bubble and generates two axial jets flowing in opposite directions. In a certain parameter range, the annular jet is accompanied by the formation of an axial jet directed away from the boundary. For large γ -values, two opposite axial jets directed towards the bubble centre are formed in the final stage of the collapse. In this case, the magnitude of the opposite forces acting on the bubble motion is, however, too small to induce a pronounced flattening of the bubble into an oblate shape which would lead to the formation of a strong annular jet. For example, for $\gamma = 2$ and $\delta = 0.195$, the horizontal axis of the expanded bubble is only about 5% longer than the vertical axis (figure 5, frame 3). Because of this small deviation from sphericity the liquid is preferentially drawn in from the sides only in a very late stage of the collapse and the bubble becomes elongated along the axis of symmetry.

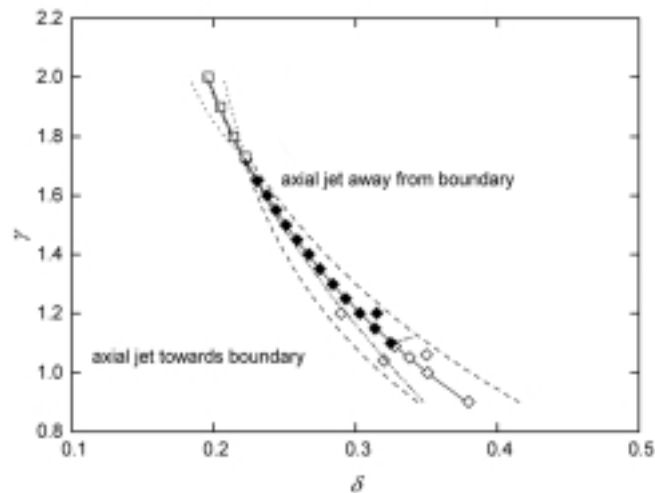


Figure 7. Jetting behaviour of a pulsating, buoyant bubble situated above a rigid boundary as a function of the stand-off γ and buoyancy parameter δ . The solid line denotes the null final Kelvin impulse state of the bubble. Open diamonds: annular jet leading to bubble splitting, filled diamonds: annular jet leading to bubble splitting, with axial liquid jet directed away from the boundary, and squares: two opposite axial liquid jets developed during bubble collapse. The dashed line surrounds the region where an annular jet leading to bubble splitting is generated, the dash and dot line the region where an annular jet and an axial jet directed away from the boundary develop during bubble collapse, and the dotted line the region where two opposite axial jets directed towards the bubble centre are observed

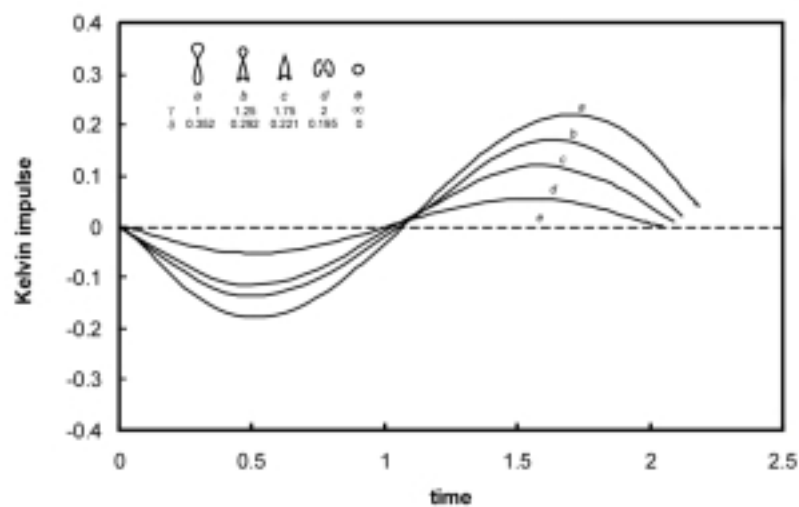


Figure 8. Kelvin impulse during the oscillation period of a bubble at the null final Kelvin impulse state. The computed bubble shapes in the final stage of the collapse are also illustrated.

It is evident that the simple analysis based on the Kelvin impulse at the end of the collapse does not portray the whole complexity of the jetting behaviour in the neighbourhood of the neutral collapse state of the bubble. It represents, however, a valuable tool in predicting the migratory characteristics of the bubble.

5. DISCUSSION

5.1. Jetting behaviour at the null final Kelvin impulse state

The results presented in the previous section revealed a very complex dynamics of a pulsating, buoyant bubble near a rigid boundary at the null final Kelvin impulse state. This includes formation of an annular jet and axial jets directed towards the bubble centre. The basic question we wish to address here is, why the bubble has so many types of behaviour for the same value of the Kelvin impulse at the conclusion of the collapse? A qualitative answer can be formulated by studying the Kelvin impulse during the collapse phase of the bubble. Figure 8 shows the variation with time of the Kelvin impulse during the first oscillation period of the bubble for different initial location of the bubble from the boundary. The starting point in explaining the mechanisms governing the jetting behaviour is given by the observation that during the collapse phase of the bubble the Kelvin impulse is directed away from the boundary. Since the buoyancy force is proportional to the bubble volume and since the pressure-gradient force is strongly manifested only in the late collapse stages, the magnitude of the buoyancy force is larger over the entire collapse phase of the bubble. (During the growth phase of the bubble the Kelvin impulse is directed towards the boundary because the bubble side nearest to the boundary moves into a region of higher relative impedance than the opposite side even though the velocities are similar. However, this feature has no consequence for jet formation). Therefore, the annular flow is developed around the lower section of the bubble, in accord with the general principles of annular jet formation discussed above. Since the Kelvin impulse increases with decreasing γ , the annular flow is initiated closer to the lower pole of the bubble with lower γ . The asymmetric annular flow results in the formation of a high-curvature region at the lower part of the bubble with the subsequent production of an axial jet directed away from the boundary. According to Lauterborn [14], jet formation can be explained by differently curved parts of the bubble surface, as the proportional relation between radius and collapse time (Rayleigh's formula) may be adopted for local radii as well. More highly curved parts of a bubble corresponding to a smaller bubble radius collapse faster than less curved parts leading to the formation of a liquid jet that threads the bubble. At very small γ -values ($\gamma \leq 1.1$), the bottom flow is inhibited by the rigid wall and the axial jet directed away from the boundary does not develop. It is interesting to note here that the formation of the axial jet directed away from the boundary would lead to a significant value of the Kelvin impulse in a very late collapse stage. This process is, however, prevented by the movement of the annular jet towards the upper bubble pole during the collapse phase so that the Kelvin impulse becomes zero at the end of the collapse. For example, when the axial jet is not developed ($\gamma = 1$), the final position of the annular jet is around the bubble equator. In contrast, for $\gamma = 1.75$ where a strong axial jet develops, the annular jet is manifested as a constriction of the polar region of the bubble on the side far from the boundary. If the calculations were to proceed further we would observe a second axial jet at the upper side of the bubble. With increasing γ , the annular flow becomes more and more symmetric leading to the formation of a prolate shape of the bubble. The top and bottom of the elongated bubble, i.e. the parts of the bubble with the highest curvature, collapses faster inducing the formation of two axial jets directed towards the bubble centre. The velocity of the upper axial jet is, however, larger than that of the lower axial jet to balance the increase of the Kelvin impulse due to the earlier formation of the lower jet. At very large γ -values, the velocity of the axial jets tends to become equal. Only in the limit $\gamma \rightarrow \infty$ and $\delta = 0$, the Kelvin impulse is zero over the whole oscillation period and the bubble keeps the spherical shape throughout its motion.

Unfortunately, despite the numerous experimental studies on the behaviour of underwater explosions near rigid boundaries [15], [16], [17], no experimental data exist with which to make a direct comparison of our simulations. This fact is not surprising taking into account how thin is the region centred around the null final Kelvin impulse state with the complex jetting behaviour. More accurate experimental studies are needed before a confirmation of the present results becomes possible. The present results suggest, however, a violent collapse of the bubble in the neighbourhood of the null final Kelvin impulse state. The most pronounced damage of the nearby boundary is likely to occur for γ -values smaller than one where the annular jet leads to bubble splitting and the formation of a high-speed axial jet directed towards the boundary. This jet is further accelerated by the shock waves emitted upon the collapse of the upper part of the bubble on the cavity closer to the boundary (see, for example, [12]). Besides this, the high pressure and temperature developed inside the collapsing bubble are also potential damage mechanisms of the nearby boundary.

5.2. A particular case: bubble motion between two parallel flat boundaries

A bubble oscillating between two parallel flat rigid boundaries is subjected to two opposite pressure-gradient forces. In this case, the null final Kelvin impulse state is obtained when the bubble is initiated at equal distance from the boundaries. It is here that the opposite pressure gradients acting on the bubble motion are of equal importance when summed over the bubble period and the Kelvin impulse is zero during both the growth and collapse phase of the bubble. Therefore, a symmetric annular flow is developed during bubble collapse. The experimental results of Chahine [10] indicate that for small γ -values the annular flow determines the formation of an equatorial jet leading to bubble splitting and the formation of two axial jets of equal velocity directed towards and away from the boundary. Furthermore, the intensity of the annular flow becomes weaker and weaker with increasing the distance between the boundaries in agreement with the present result illustrated in figure 6. It is expected that for a sufficiently large distance between the boundaries the bubble achieves a prolate shape during collapse leading to the formation of two axial jets of equal velocity directed towards the bubble centre. Although no direct observation is available in literature, the numerical calculations of Shima and Sato [18] indicates that two opposite axial jets can be formed when a bubble with an initially prolate spheroidal shape collapses between two flat rigid boundaries. It should be noted here that an experimental evidence of this feature seems to be a real challenge since, as shown in figure 5, the axial jets are formed during the very late stage of the collapse where the bubble is at the minimum volume.

5.3. A more complex case: bubble motion near an elastic boundary

The bubble dynamics near an elastic wall also belongs to the class of motion in the presence of opposite pressure gradients. As in the case of a rigid wall, the bubble oscillation is associated with a pressure gradient directed towards the wall due to the low pressure region between bubble and wall developed during bubble collapse. Unlike the rigid wall, however, the material is compressed during bubble expansion, it rebounds, and thus creates a flow and a pressure gradient directed away from the wall. Recent experimental results [12] indicate that a dominant feature of the bubble behaviour at the neutral collapse state is the formation of an asymmetric annular jet around the bubble part closer to the elastic wall. This indicates, according to the present analysis, that the Kelvin impulse is directed away from the boundary during bubble collapse. This assertion is supported by the observation that the rebound of the elastic boundary starts before the bubble reaches its maximum expansion. The magnitude of the pressure gradient induced by the rebounding boundary is thus larger than that of the pressure gradient directed towards the wall which is strongly manifested only during the very late stage of the collapse and, consequently, the Kelvin impulse is directed away from the elastic wall during the whole collapse phase of the bubble. Furthermore, the movement of the annular jet towards the opposite bubble pole during bubble collapse was also observed, in agreement with the results of the present calculations. The particularity of this case is the suppression of the axial jet directed away from the boundary at the neutral collapse state of the bubble. This is due, on one hand, to the uplifting of the elastic wall during bubble collapse which keeps the bubble in close proximity to the wall even in a very late stage of its collapse and, on the other hand, to the jet-like ejection of the boundary material which penetrates the bubble pole facing the elastic wall. With increasing the stiffness of the boundary, the amplitude of the boundary deformation becomes smaller leading to a smaller magnitude of the Kelvin impulse during bubble collapse and to the formation of a more symmetric and weaker annular jet during bubble collapse. Although this is a prerequisite for the formation of two axial jets directed towards bubble centre, this case was not observed in experiment. It should be noted, however, that the experiment was conducted for values of the static elastic modulus of the material of up to 2 MPa. Therefore, further careful experiments using stiffer materials need to be done to validate this theoretical result.

6. CONCLUSIONS

The dynamics of a pulsating, buoyant bubble near a rigid boundary at the null final Kelvin impulse state is investigated numerically by using a boundary integral method. This case is particularly interesting because the opposite forces acting on the bubble, namely, the buoyancy force directed away from the boundary and the pressure-gradient force directed towards the boundary, are of equal importance when

summed over the bubble period at the end of the bubble collapse. The bubble dynamics shows a large variation in the jetting behaviour depending on the initial distance between bubble and boundary. The complex behaviour is attributed to a difference between the strength of the opposite forces during the collapse phase of the bubble.

The dominant feature of the bubble dynamics is the formation of an asymmetric annular flow around the lower part of the bubble during collapse. The annular flow is a result of the oblate spheroidal shape of the bubble at its maximum expansion, while the asymmetry of the flow is a consequence of a relatively larger magnitude of the buoyancy force in the initial stage of the collapse. This results in a higher curvature of the lower bubble wall and subsequent formation of a high-speed axial liquid jet directed away from the boundary. In a later collapse stage the annular jet moves towards the upper part of the bubble to prevent the increase of the Kelvin impulse induced by the formation of the axial jet. At very small γ -values, the formation of the axial jet is inhibited by the boundary and only the annular jet is manifested during bubble collapse. At very large γ -values, the bubble behaviour is characterized by the formation of two axial jets directed towards the bubble centre. This is a consequence of the prolate spheroidal shape of the collapsing cavity which, in turn, is caused by a more symmetric but weaker annular flow in the initial stage of the collapse.

The present results also demonstrates that the Kelvin impulse provides accurate predictions of the jetting behaviour even in the neighbourhood of the neutral collapse state of a bubble. The direction of the Kelvin impulse during the collapse phase of the bubble determines the position of the annular jet in the initial stage of the collapse while its magnitude indicates the degree of asymmetry and the intensity of the annular jet. These are the essential factors in estimating the final fate of a bubble situated in opposing pressure gradients and near the neutral collapse state of the bubble. Far from this state, the final Kelvin impulse is an extremely valuable and accurate tool in predicting the migratory characteristics of the bubble and the direction of the axial jet developed during bubble collapse.

ACKNOWLEDGEMENTS

This study has been partially supported by EPSRC (grant GR/N36868/01) and CNCSIS (Grant 122/2003).

REFERENCES

1. RAYLEIGH, LORD, On the pressure developed in a liquid during the collapse of a spherical cavity. *Philosophical Magazine*, **34**, pp. 94-98, 1917
2. PROSPERETTI, A., LEZZI, A., Bubble dynamics in a compressible liquid. Part 1. First order theory. *Journal of Fluid Mechanics*, **168**, pp. 457-478, 1986.
3. KORNFELD, M., SUVOROV, L., On the destructive action of cavitation. *Journal of Applied Physics*, **15**, pp. 495-506, 1944.
4. PLESSET, M.S., CHAPMAN, R.B., Collapse of an initially spherical vapour cavity in the neighbourhood of a solid boundary. *Journal of Fluid Mechanics*, **47**, pp. 283-290, 1971.
5. BLAKE, J.R., TAIB, B.B., DOHERTY, G., Transient cavities near boundaries. Part 1. Rigid boundary. *Journal of Fluid Mechanics*, **170**, pp. 479-497, 1986.
6. VOGEL, A., LAUTERBORN, W., TIMM, R., 1989 Optical and acoustic investigations of the dynamics of laser-produced cavitation bubbles near a solid boundary. *Journal of Fluid Mechanics*, **206**, pp. 299-338, 1989.
7. BEST, J.P., KUCERA, A., A numerical investigation of non-spherical rebounding bubbles. *Journal of Fluid Mechanics*, **245**, pp. 137-154, 1992.
8. COLE, R.H., *Underwater explosions*. Princeton University Press, 1948.
9. BENJAMIN, T.B., ELLIS, A.T., The collapse of cavitation bubbles and the pressures thereby produced against solid boundaries. *Philosophical Transactions of the Royal Society London A*, **260**, pp. 221-240, 1966.
10. CHAHINE, G.L., Experimental and asymptotic study of nonspherical bubble collapse. *Applied Scientific Research*, **38**, pp. 187-197, 1982.
11. ROBINSON, P.B., BLAKE, J.R., Dynamics of cavitation bubble interactions. In *Proceedings IUTAM Symposium "Bubble Dynamics and Interface Phenomena"* (ed. J. R. Blake et al.), pp. 55-64, 1994, Kluwer.
12. BRUJAN, E.A., NAHEN, K., SCHMIDT, P., VOGEL, A., Dynamics of laser-induced cavitation bubbles near elastic boundaries: Influence of the elastic modulus. *Journal of Fluid Mechanics*, **433**, pp. 283-314, 2001.
13. GODWIN, R.P., CHAPYAK, E.J., NOACK, J., VOGEL, A., Aspherical bubble dynamics and oscillation times. *SPIE Proceedings*, **3601**, pp. 225-237, 1999.

14. 14. LAUTERBORN, W., Cavitation bubble dynamics-new tools for an intricate problem. *Applied Scientific Research*, **38**, pp. 165-178, 1982.
15. 15. MENON, S., LAL, M., On the dynamics and instability of bubble formed during underwater explosions. *Experimental Thermal Fluid Science*, **16**, pp. 305-321, 1998.
16. 16. KIRA, A., FUJITA, M., ITOH, S., Underwater explosion of spherical explosives. *Journal of Material Processing and Technology*, **85**, pp. 64-68, 1999.
17. 17. RAJENDRAN, R., NARASIMHAN, K., Linear elastic response of plane plates subjected to underwater explosions. *International Journal of Impact Engineering*, **25**, pp. 493-506, 2001.
18. 18. SHIMA, A., SATO, Y., The collapse of a bubble between narrow parallel plates (The case where a bubble is attached to a solid wall). *Reports Institute High Speed Mechanics, Tohoku University*, **49**, pp. 1-21, 1984.

Received November 20, 2003